crystals

MDPI

Article

A Theoretical Model of Quasicrystal Resonators: A Guided Optimization Approach

Libin Cui [1], Anwer Hayat [1], Linzheng Lv [2], Zhiyang Xu [1] and Tianrui Zhai [1,*]

[1] College of Physics and Optoelectronics, Faculty of Science, Beijing University of Technology, Beijing 100124, China; cuilb_68@bjut.edu.cn (L.C.); anwerhayatnoor@gmail.com (A.H.); xu.zhiyang@bjut.edu.cn (Z.X.)

[2] College of Continuing Education, Beijing University of Technology, Beijing 100124, China; lvlinzheng@bjut.edu.cn

* Correspondence: trzhai@bjut.edu.cn; Tel.: +86-010-6739-2184

Abstract: Fibonacci-spaced defect resonators were analytically investigated by cavity coupling, which exhibited a series of well-defined optical modes in fractals. The analytic model can be used to predict the output performance of microcavity lasers based on Fibonacci-spaced defect resonators, such as the mode number, resonant frequency, and Q factor. All results obtained by the analytical solution are in good consistency with that obtained by the finite-difference time-domain method. The simulation result shows that the Q factor of the resonant modes would increase dramatically with the appearance of narrower optical modes. The proposed theoretical model can be used to inversely design high performance polymer lasers based on the Fibonacci-spaced defect resonators.

Keywords: quasicrystal resonator; analytic model; cavity coupling

Citation: Cui, L.; Hayat, A.; Lv, L.; Xu, Z.; Zhai, T. A Theoretical Model of Quasicrystal Resonators: A Guided Optimization Approach. *Crystals* **2021**, *11*, 749. https://doi.org/10.3390/cryst11070749

Academic Editor: Valentina Domenici

Received: 12 May 2021
Accepted: 23 June 2021
Published: 26 June 2021

1. Introduction

The discovery of quasicrystals in condensed matter has revolutionized solid-state physics [1–3]. During the last few decades, photonic quasicrystals have been extensively discussed and studied [4–9]. Quasiperiodic structures are natural intermediate cases between periodicity and randomness, which provide more optical design possibilities and richness in the engineering performance of the optical devices. The design of optical devices based on the quasiperiodic structures can achieve a better performance than periodic ones for some specific optical applications, which opens new avenues in the quest for high performance optical devices [10–16].

One-dimensional (1D) optical quasicrystal lattices composed of multilayer stacks have two different dielectrics of permittivity, ε_1 and ε_2, arranged in deterministic generation rule, which exhibit long-range order but lack of translational symmetry. All these structures exhibit self-similar properties.

In the case of 1D optical quasicrystals the quasicrystalline long-range order results in a pseudogap similar to the bandgap of photonic crystals, while the lack of periodicity in the quasicrystal results in critically localized optical modes similar to the localization in the random systems; in other words, it can be considered as a defect effect. This leads to the appearance of allowed optical modes inside the forbidden 1D pseudogap. The optical modes exhibit fractal self-similar patterns in the transmission spectra that stem from the self-similarity of the underlying structure [17–19]. High Q-factor resonators can be attained due to the splitting and sharpness of the previous modes from the well-defined self-similar feature [20]. Moreover, the progressive fragmentation of the frequency spectrum gives rise to a series of optical modes, which means that in the limit of a large sample size their spectra become singular continuous, which provide many additional Bragg resonances for feedback, leading to a multicolor laser at arbitrarily chosen frequencies within the gain bandwidth [21,22].

The optical modes inside quasicrystals are confined in space but decay weakly rather than exponentially [23–25], which leads to the crosstalk between modes in the energy spectra and it is difficult to realize single-mode control. This is commonly referred to as the "non-resonant" case [4,5,26]. Resonant quasiperiodic multi-quantum-well stacks were proposed [27–29], which show a shorter emission lifetime and higher photoluminescence emission intensity than that in non-resonant conditions.

How are resonator properties such as wavelength, number of modes and output controlled by the quasiperiodicity? Many important concepts that are related to crystals, such as band structure, Bloch theorem, Brillouin zone, etc., are invalid in quasicrystals. The optical behavior of 1D optical quasicrystal lattices can be investigated numerically using the transfer matrix method [26,30–32] and the plane wave method [33]. However, the numerical solutions are not intuitive.

In this paper, we proposed a resonant Fibonacci-spaced multiple-defect-cavity structures, which exhibits properties of self-similar optical modes with a series of well-separated peaks. At the resonant condition, the system is resonant and strongly coupled. When there is an increase in the generation order, very narrow optical modes would appear and the Q factor of the resonant modes would increase exponentially with mode splitting. We developed a general theoretical model of the 1D quasicrystal resonator based on the coupled mode theory. The mode splitting, number and frequency of the resonant modes were explained qualitatively by an analytical solution. The theoretical model is completely consistent with the finite difference time domain (FDTD) simulation. We also demonstrate the inverse design of 1D Fibonacci-spaced resonators for the desired wavelength and amplitude of optical modes which can realize the broad color gamut laser display.

2. Theoretical Analysis

2.1. Theoretical Model of 1D Fibonacci-Spaced Defect Resonators

One dimensional resonant Fibonacci quasicrystals systems based on multiple defect cavities with two different interdefect distances satisfy the Fibonacci-chain rule between the long and short interdefect distances, as shown in Figure 1. The separations between the defect cavities are denoted by short(S) and long(L), respectively. The Fibonacci chain ($LSLLSLSL\ldots$) follows the construction rule that the next complete sequence is the present sequence plus the previous sequence, marking the first sequence as S and the second as L.

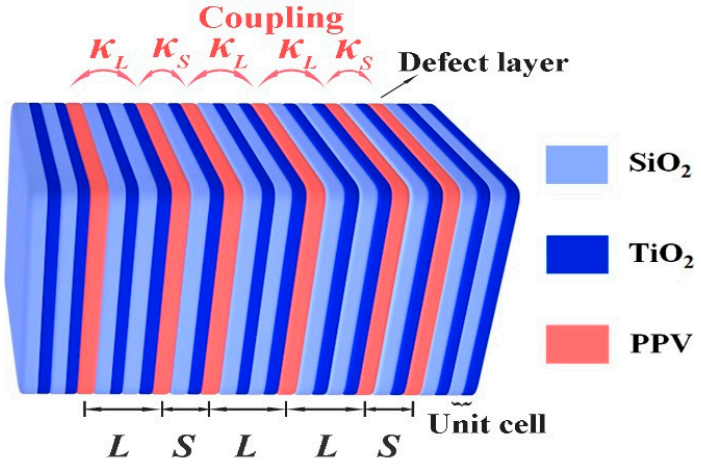

Figure 1. Scheme of 1D Fibonacci-spaced defect resonators. The PPV layers are inserted in the period stacks of SiO_2/TiO_2 structures, in which the PPV acts as both the defect cavity and the gain medium.

In the defect cavity, light is confined in a small volume, which enhances light–matter interactions and favors the laser behavior. The high-Q resonance and wavelength size of defect cavity make it extremely suitable for creating the coupled microcavity arrays. The widths of the interdefect cavity were determined from the resonant Bragg conditions,

specifying the constructive interference of the waves reflected from the multiple defect cavities at the excitonic resonance.

The resonant electric field of each defect microcavity could enter into the other's field with a coupling constant κ. Similarly, the amount of the coupling can be defined by taking the overlap integral of the modes from the electric field as it enters into the other's field with a coupling strength. We have developed our theoretical model based on the coupled-wave theory. When the coupling effect between the cavities is ignored, there will be one resonant mode in the above system under the resonant condition. The field amplitude in the microcavity evolves over time as $exp(-i\omega t)$, therefore, the dynamic equations for resonance amplitudes can be written as: $\frac{da}{dt} = -i\omega a$, where a is the field amplitude in the microcavity, and ω is the resonant frequency [34]. Let us consider the cavity mode coupling effect between the cavities, as shown in Figure 1. We ignore the coupling between the non-adjacent cavities. According to the coupled-wave theory, the dynamic equations for the nth resonant cavity can be written in the following form [35]:

$$\frac{da_n}{dt} = -i\omega_n a_n + i\kappa_{n-1\ n} a_{n-1} + i\kappa_{n+1\ n} a_{n+1} \tag{1}$$

where a_n is the mode amplitude of the nth resonator, $\kappa_{n-1\ n}$ and $\kappa_{n+1\ n}$ present the coupling coefficients of the modes $n-1$ and $n+1$ coupled to the mode n, respectively. The Fourier transform of a_n is

$$a_n(t) = \int A_n(\omega) exp(-i\omega t) d\omega \tag{2}$$

Inserting the value of Equation (2) into Equation (1) and considering all N resonators, after solving, the coupling equations in the frequency domain for the given system can be expressed as:

$$\begin{bmatrix} \omega_1 - \omega_0 & -\kappa_{21} & 0 & \cdots & 0 \\ -\kappa_{12} & \omega_2 - \omega_0 & -\kappa_{32} & \cdots & 0 \\ \cdots & \cdots & \cdots & \cdots & \cdots \\ 0 & 0 & \cdots & \omega_{N-1} - \omega_0 & -\kappa_{NN-1} \\ 0 & 0 & \cdots & -\kappa_{N-1N} & \omega_N - \omega_0 \end{bmatrix} \begin{bmatrix} A_1 \\ A_2 \\ \cdots \\ A_{N-1} \\ A_N \end{bmatrix} = 0 \tag{3}$$

where $A_1, A_2 \cdots A_N$ are the complex amplitude of the N resonant cavities and ω_0 is the unperturbed Bragg frequency. Therefore, the above equations will lead a nonzero solutions when the determinant of the coefficient of equations D_N equals zero. Considering the coupling coefficient between the two cavities is irrelevant to the direction of coupling. In the two opposite directions, we suppose $\kappa_{ij} = \kappa_{ji} = \kappa_i$, D_N can be expressed as:

$$D_N = \begin{vmatrix} \omega_1 - \omega_0 & -\kappa_1 & 0 & \cdots & 0 \\ -\kappa_1 & \omega_2 - \omega_0 & -\kappa_2 & \cdots & 0 \\ \cdots & \cdots & \cdots & \cdots & \cdots \\ 0 & 0 & \cdots & \omega_{N-1} - \omega_0 & -\kappa_{N-1} \\ 0 & 0 & \cdots & -\kappa_{N-1} & \omega_N - \omega_0 \end{vmatrix} = 0 \tag{4}$$

According to Equation (4), we construct the coupling matrix as follows:

$$C_N = \begin{vmatrix} 0 & \kappa_1 & 0 & \cdots & 0 \\ \kappa_1 & 0 & \kappa_2 & \cdots & 0 \\ \cdots & \cdots & \cdots & \cdots & \cdots \\ 0 & 0 & \cdots & 0 & \kappa_{N-1} \\ 0 & 0 & \cdots & \kappa_{N-1} & 0 \end{vmatrix} \tag{5}$$

Equation (5) implies that diagonal elements are zero because the mode of the one cavity is not coupled to itself for the off diagonal elements $\kappa_{ij} = 0$, except $j = i \pm 1$, because coupling between the non-adjacent cavities should not be considered.

By comparing Equation (4) and Equation (5), we can obtain $D_N = |(\omega - \omega_0)E - C_N|$, where E is the unit matrix. Therefore, $\omega - \omega_0$ is the eigenvalue of C_N. As described in Equation (5), C_N is a real symmetric matrix, $(C_N)^T = C_N$. For N we can obtain the eigenvalue $\omega_1 - \omega_0$, $\omega_2 - \omega_0$ ... $\omega_N - \omega_0$ from the symmetry of C_N. It can be further proved by the matrix theory that these N eigenvalues are different. (The detailed derivation process is described in Appendix A). Thus, the cavity coupled modes split into the N resonance modes.

Based on the well-known matrix theory, we can obtain the resonance frequencies for the N defect microcavities arranged following the Fibonacci sequence as described in Figure 1. The coupling coefficients between the cavities with short and long separations are denoted by κ_S and κ_L, respectively. Therefore, Equation (4) can be written as:

$$D_N = \begin{vmatrix} \omega_1 - \omega_0 & -\kappa_L & 0 & \cdots & 0 \\ -\kappa_L & \omega_2 - \omega_0 & -\kappa_S & \cdots & 0 \\ \cdots & \cdots & \cdots & \cdots & \cdots \\ 0 & 0 & \cdots & \omega_{N-1} - \omega_0 & -\kappa_{N-1} \\ 0 & 0 & \cdots & -\kappa_{N-1} & \omega_N - \omega_0 \end{vmatrix} = 0 \quad (6)$$

After solving the linear equations, the resonant frequencies can be obtained. D_N can be expressed as the following recursive relation (See Appendix B for detailed derivation). Note that κ_{N-1} depends on the parity of N.

$$D_N = (\omega - \omega_0)D_{N-1} - \kappa_{N-1}^2 D_{N-2} \quad (7)$$

Once we know both D_2 and D_3, D_N can be extracted step by step using Equation (7).

2.2. Analytical Results and Discussion

We can figure out all the resultant resonant frequencies from the solution of Equation (6) and some results are described in Table 1.

Table 1. The frequencies of the coupled defect mode for $N = 1, 2, 3, 5$, respectively.

The Defect Numbers	The Frequencies of the Coupled Defect Modes
1	$\omega = \omega_0$
2	$\omega = \omega_0 \pm \Delta\omega = \omega_0 \pm \kappa_L$
3	$\omega = \omega_0, \omega = \omega_0 \pm \Delta\omega = \omega_0 \pm \sqrt{\kappa_S^2 + \kappa_L^2}$
5	$\omega = \omega_0, \omega = \omega_0 \pm \Delta\omega = \omega_0 \pm \kappa_L, \omega = \omega_0 \pm \Delta\omega = \omega_0 \pm \sqrt{\kappa_S^2 + 2\kappa_L^2}$

We noticed in the analytical solution that the resonant frequencies are distributed symmetrically about ω_0 and can be evaluated from the coupling coefficient κ_S and κ_L. If $\kappa_S = \kappa_L$, it is referred to a as periodic defect cavities chain, which has been studied in our previous work [36]. Similarly, the Fibonacci-spaced defect resonators exhibit unusual properties, which are very different from those of periodic and random systems, as we can see in Figure 2a, where we plot the evolution of resonant modes as generation order increase, which show self-similar properties of typical Cantor sets.

It could be proved by the matrix theory there exist a limit value for the maximum and minimum resonant frequencies in the above analytical solution. This means that in a limited spectral region the spectra are highly fragmented. For large generation order, the line width of the resonant modes decreases dramatically, which results in resonators with high Q-factors.

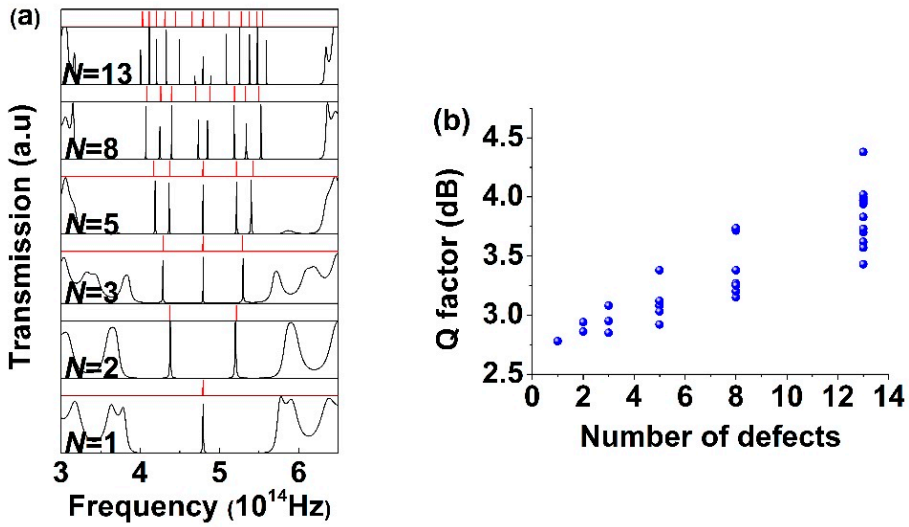

Figure 2. (**a**) Comparison of resonant frequencies of the Fibonacci-spaced defect resonators obtained from the theoretical model developed (the red line) and the simulation using FDTD (the black line) with different generation order for $\kappa_S = 0.42$, $\kappa_L = 0.27$. The results agree well, and the discrepancies are expected to vanish if the first and last coupling coefficients are modified due to external losses. (**b**) Q factor increases exponentially with mode splitting.

Due to their highly fragmented frequency spectra, a Fibonacci-spaced chain of defect cavities offers more resonant frequencies than periodic ones in a given frequency range for a given system length, which provides a higher degree of design and tuning flexibility. The analytical solution of the proposed theoretical model can be used to customize high performance microcavity resonators and it can be made via inverse design. The theoretical mode can also be extended to predict the characteristics of 2D quasiperiodic structures.

3. Simulation and Validation

To validate the theoretical analysis, we compare the theoretical results to the FDTD simulations. In the simulation, the refractive indices of SiO_2 and TiO_2 were chosen as 1.54 and 2.5, respectively, which were measured by a spectroscopic ellipsometer (ESNano, Ellitop). The thickness of the SiO_2/TiO_2 layer was 90/70 nm. The refractive index and the thickness of the MDMO-PPV (defect/gain layer) were about 1.67 and 94 nm, respectively. The important parameters were optimized by FDTD, so that the photonic band gap overlapped almost completely with the emission spectrum of MEMO-PPV, and the unperturbed defect mode frequency is exactly at the center of band-gap of the 1D photonic structure.

We found an excellent agreement in the resonant frequencies by comparing the results of the analytical model based on the coupling mode effect with FDTD simulation, as shown in Figure 2a. The deviations between the theory and the simulation are from the coupling of two cavities on both sides to the outside world. We expect this discrepancy vanish if the external losses are modified in the first and last coupling coefficients.

It can be observed from Figure 2a that every mode of any hierarchy will split into submodes to form the Cantor spectrum. In the third hierarchy there are three modes: the mode on the both sides will further split into submode for the global structure, and the middle mode will also split in the same manner for next stage. Thus, it turns out that the Fibonacci-spaced defect resonators have a perfect self-similar spectrum. The Q factor of the resonant modes would increase exponentially with the appearance of narrower optical modes, as shown in Figure 2b. Considering only the resonant modes in the center of the band, the Q value increases from 480 for $N = 1$ to 23,960 for $N = 13$, where the size of the device increases from 1.694 to 5.862 μm.

4. Inverse Design of Laser Resonators Based on the Fibonacci-Spaced Defect Resonators

Some features of the regular quasicrystals are not required for the operation of microcavity lasers. According to the analytical model, the regular quasicrystals can be modified to be an ideal resonator for microcavity lasers. For example, the mode splitting provides a simple, flexible and versatile approach for the design of high performance resonators [36–40]. It would allow us to engineer the behavior of the cavity mode simply by tailoring the separation and size of the defects. Here, the ratio $\alpha = \frac{L}{S}$ is arbitrary. For $L = S$ the structure becomes periodic and for τ equal to the golden mean 1.618, it becomes the canonical Fibonacci chain [41]. The simulation results show that $\Delta\omega$, which refers to frequency detuning from ω_0 due to coupling, decreases exponentially with increasing the ratio α, as shown in Figure 3.

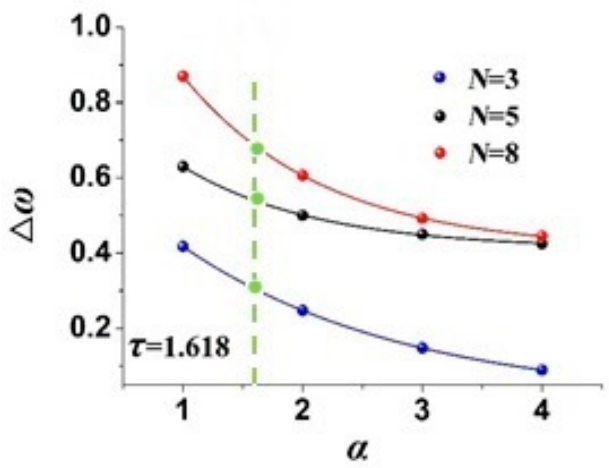

Figure 3. The relation between $\Delta\omega$ and α for $N = 3, 5, 8$. The dotted line indicates the positions on the curve at $\tau = 1.618$.

According the relation between $\Delta\omega$ and α and the analytical solutions mentioned above, we can optimize 1D quasicrystal resonators to obtain target optical modes at arbitrary positions in a broad spectral range.

In this section, we have studied inverse design of the 1D quasicrystals resonators to obtain desired laser emission, as shown in Figure 4. By adjusting the separation of the defects in above model, the optical modes can be fine-tuned across a broad-spectrum range, as shown in Figure 4a. Organic polymers have broad emission spectrum, which demonstrates excellent features in flexible spectrum modulation. It has been reported [42,43] that the intensity of the band-gap modes can be adjusted by controlling the phase shift of both reflecting facets. In Figure 4b, we have demonstrated the effect on the intensity of optical modes in the band-gap by changing the number of boundary layers. Based on the analytic model, the number of optical modes can be predicted, which corresponds to the number of defects, as shown in Figure 4c. The wavelength and intensity of the output emissions are calculated as points located in the CIE chromaticity diagram in Figure 4d. Thus, the CIE chromaticity demonstrates the output of the laser with broad color gamut.

Note that there is a slight difference between the resonant frequency of Fibonacci-spaced defect resonators obtained from the theoretical model and that obtained from FDTD, especially for high generation orders. It can be attributed to the fact that the coupling between non-adjacent cavities is not considered in the proposed method. Even so, the developed analytical model can be extended to a more general case of aperiodic plasmonic systems, which provides a simple and efficient route towards designing real systems with flexible, multispectral optical responses. It opens a new avenue in the quest for high performance optical devices.

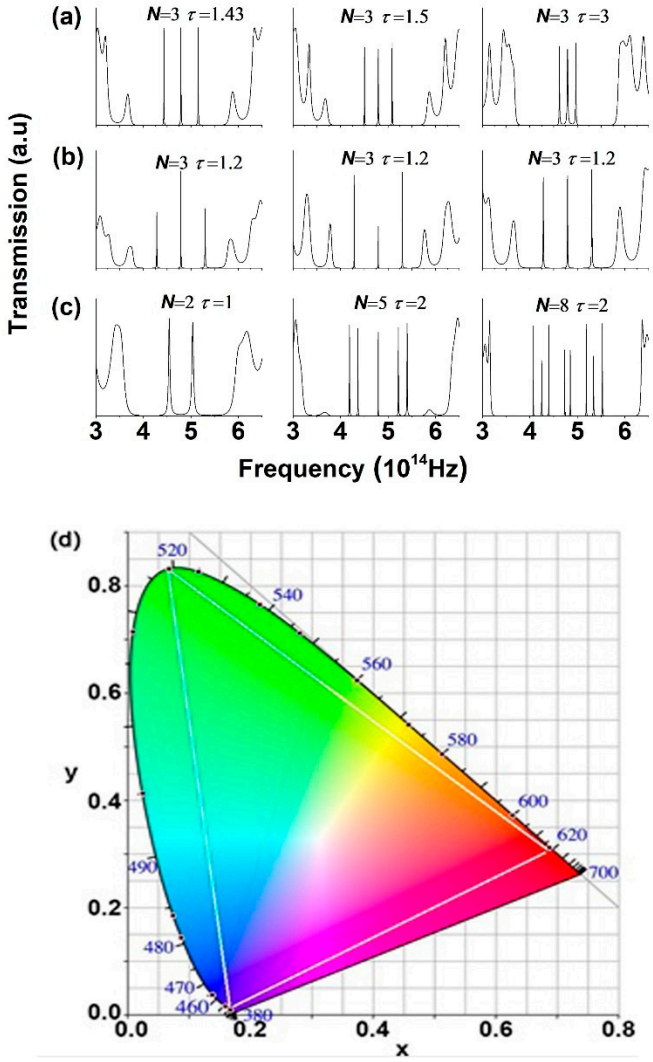

Figure 4. (**a**) Modes splitting for $N = 3$ with $\tau = 3$, 1.5, 1.43. (**b**) Intensity of optical modes for different boundary layers. (**c**) The number of optical modes for different number of defects. (**d**) Schematic diagram of the emission spectra for the R, G and B components.

5. Conclusions

In conclusion, we have presented 1D quasicrystal resonators which exhibit progressive fragmentation of the frequency spectrum as generation order increases and gives rise to quasicontinuous but well-defined optical modes in the limit of large sample size. The analytical solution of the proposed theoretical model provides precise control on single- or multifrequency across a broad spectral range, which can be used in the polymer laser-based display with broad color gamut and also can meet the operating requirements of high-resolution spectroscopy.

Author Contributions: Conceptualization, L.C. and T.Z.; Methodology, L.C. and L.L.; Validation, L.C. and T.Z.; Formal Analysis, L.C. and L.L.; Investigation, L.C. and Z.X.; Writing—Original Draft Preparation, L.C.; Writing—Review and Editing, L.C., A.H., and T.Z.; Supervision, T.Z.; Project Administration, T.Z.; Funding Acquisition, T.Z. All authors have read and agreed to the published version of the manuscript.

Funding: Beijing Natural Science Foundation (Z180015); National Natural Science Foundation of China (61822501).

Institutional Review Board Statement: Not applicable.

Informed Consent Statement: Not applicable.

Data Availability Statement: Data sharing not available.

Conflicts of Interest: The authors declare no conflict of interest.

Appendix A

In the first step, keeping in view the concept of matrix theory, if C_N is a real symmetric matrix, it can be deduced that C_N has N real eigenvalues. In the second step, if we have $D_N = (\omega - \omega_0)E - C_N = (d_{ij})$, then the cofactor of d_{N1} can be arranged in the following form:

$$\begin{vmatrix} -\kappa_1 & 0 & \cdots & 0 & 0 \\ \omega-\omega_0 & -\kappa_2 & \cdots & 0 & 0 \\ \cdots & \cdots & \cdots & \cdots & \cdots \\ 0 & 0 & \cdots & -\kappa_{N-2} & 0 \\ 0 & 0 & \cdots & \omega-\omega_0 & -\kappa_{N-1} \end{vmatrix}_{N-1} = (-1)^{N-1}\kappa_1\kappa_2\cdots\kappa_{N-1} \neq 0 \quad \text{(A1)}$$

Thus, the rank of D_N is greater than or equal to 1, that is $R(D_N) \geq N-1$. On the other hand, $R(D_N) \leq N-1$ because $\omega - \omega_0$ is the eigenvalue of C_N. Therefore, we can obtain $R(D_N) = N-1$ for any eigenvalue of C_N. From $R(D_N) = N-1$, we can derive that N real eigenvalues of C_N are different. In summary, it can be concluded that C_N has N different real eigenvalues.

Appendix B

D_N is the determinant of tridiagonal matrix in Equation (6). It can be written as:

$$D_N = \begin{vmatrix} \omega-\omega_0 & -\kappa_L & 0 & \cdots & 0 \\ -\kappa_L & \omega-\omega_0 & -\kappa_S & \cdots & 0 \\ \cdots & \cdots & \cdots & \cdots & \cdots \\ 0 & 0 & \cdots & \omega-\omega_0 & -\kappa_{N-1} \\ 0 & 0 & \cdots & -\kappa_{N-1} & \omega-\omega_0 \end{vmatrix} =$$

$$(\omega-\omega_0)\begin{vmatrix} \omega-\omega_0 & -\kappa_L & 0 & \cdots & 0 \\ -\kappa_L & \omega-\omega_0 & -\kappa_S & \cdots & 0 \\ \cdots & \cdots & \cdots & \cdots & \cdots \\ 0 & 0 & \cdots & \omega-\omega_0 & -\kappa_{N-2} \\ 0 & 0 & \cdots & -\kappa_{N-2} & \omega-\omega_0 \end{vmatrix}_{N-1} \quad \text{(A2)}$$

$$-\kappa_{N-1}^2\begin{vmatrix} \omega-\omega_0 & -\kappa_L & 0 & \cdots & 0 \\ -\kappa_L & \omega-\omega_0 & -\kappa_S & \cdots & 0 \\ \cdots & \cdots & \cdots & \cdots & \cdots \\ 0 & 0 & \cdots & \omega-\omega_0 & -\kappa_{N-3} \\ 0 & 0 & \cdots & -\kappa_{N-3} & \omega-\omega_0 \end{vmatrix}_{N-2}$$

Thus, from Equation (A2), D_N can be expressed as the following recursive relation:

$$D_N = (\omega-\omega_0)D_{N-1} - \kappa_{N-1}^2 D_{N-2}$$

where D_{N-1} and D_{N-2} are the determinant of the bottom-right $(N-1)\times(N-1)$ and $(N-2)\times(N-2)$ submatrix of D_N respectively.

References

1. Shechtman, D.; Blech, I.; Gratias, D.; Cahn, J.W. Metallic phase with long-range orientational order and no translational symmetry. *Phys. Rev. Lett.* **1984**, *53*, 1951–1953. [CrossRef]
2. Kraus, Y.E.; Aahini, Y.; Ringel, Z.; Verbin, M.; Zilberberg, O. Topological states and adiabatic pumping in quasicrystals. *Phys. Rev. Lett.* **2012**, *109*, 106402. [CrossRef] [PubMed]

3. Bourne, C.; Prodan, E. Non-commutative chern numbers for generic aperiodic discrete systems. *J. Phys. A Math. Theor.* **2018**, *51*, 235202. [CrossRef]
4. Kohmoto, M.; Sutherland, B.; Iguchi, K. Localization of optics: Quasiperiodic media. *Phys. Rev. Lett.* **1987**, *58*, 2436–2438. [CrossRef] [PubMed]
5. Nguyen, T.D.; Nahata, A.; Vardeny, Z.V. Measurement of surface plasmon correlation length differences using Fibonacci deterministic hole arrays. *Opt. Express* **2012**, *20*, 15222–15231. [CrossRef]
6. Vitiello, M.S.; Nobile, M.; Ronzani, A.; Tredicucci, A.; Castellano, F.; Talora, V.; Li, L.; Linfield, E.H.; Davies, A.G. Photonic quasi-crystal terahertz lasers. *Nat. Commun.* **2014**, *5*, 5884. [CrossRef]
7. Boguslawski, M.; Lučić, N.M.; Diebel, F.; Timotijević, D.V.; Denz, C.; Jović Savić, D.M. Light localization in optically induced deterministic aperiodic Fibonacci lattices. *Optica* **2016**, *3*, 711–717. [CrossRef]
8. Schokker, A.H.; Koenderink, A.F. Lasing in quasi-periodic and aperiodic Plasmon lattices. *Optica* **2016**, *3*, 686–693. [CrossRef]
9. Negro, L.D.; Chen, Y.; Sgrignuoli, F. Aperiodic photonics of elliptic curves. *Crystals* **2019**, *9*, 482. [CrossRef]
10. Moretti, L.; Rea, I.; Stefano, L.D.; Rendina, I. Periodic versus aperiodic: Enhancing the sensitivity of porous silicon based optical sensors. *Appl. Phys. Lett.* **2007**, *90*, 191112. [CrossRef]
11. Makarava, L.N.; Nazarov, M.M.; Ozheredov, I.A.; Shkurinov, A.P.; Smirnov, A.G.; Zhukovsky, S.V. Fibonacci-like photonic structure for femtosecond pulse compression. *Phys. Rev. E* **2007**, *75*, 036609. [CrossRef] [PubMed]
12. Macia, E. Exploiting aperiodic designs in nanophotonic devices. *Rep. Prog. Phys.* **2012**, *75*, 036502. [CrossRef]
13. Negro, L.D.; Boriskina, S.V. Deterministic aperiodic nanostructures for photonics and plasmonics applications. *Laser Photonics Rev.* **2012**, *6*, 178–218. [CrossRef]
14. Barriuso, A.G.; Monzon, J.J.; Yonte, T.; Felipe, A.; Soto, L. Omnidirectional reflection from generalized Fibonacci quasicrystals. *Opt. Express* **2013**, *21*, 30039–30053. [CrossRef]
15. Biasco, S.; Li, L.; Linfield, E.; Davies, A.; Vitiello, M. Multimode, aperiodic terahertz surface-emitting laser resonators. *Photonics* **2016**, *3*, 32. [CrossRef]
16. Davis, M.S.; Zhu, W.; Xu, T.; Lee, J.K.; Lezec, H.J.; Agrawal, A. Aperiodic nanoplasmonic devices for directional colour filtering and sensing. *Nat. Commun.* **2017**, *8*, 1347. [CrossRef]
17. Vasconcelos, M.S.; Albuquerque, E.L. Transmission fingerprints in quasiperiodic dielectric multilayers. *Phys. Rev. B* **1999**, *59*, 11128–11131. [CrossRef]
18. Thiem, S.; Schreiber, M. Local symmetry dynamics in one-dimensional aperiodic lattices: A numerical study. *Nonlinear Dynam.* **2014**, *78*, 71–91.
19. Tanese, D.; Gurevich, E.; Baboux, F.; Jacqmin, T.; Lemaˆıtre, A.; Galopin, I.S.E.; Amo, A.; Bloch, J.; Akkermans, E. Fractal energy spectrum of a polariton gas in a Fibonacci quasi-periodic potential. *Phys. Rev. Lett.* **2014**, *112*, 146404–146409. [CrossRef]
20. Karman, G.P.; Mcdonald, G.S.; New, G.H.C.; Woerdman, J.P. Fractal modes in unstable resonators. *Nature* **1999**, *402*, 138. [CrossRef]
21. Mahler, L.; Tredicucci, A.; Beltram, F.; Walther, C.; Faist, J.; Beere, H.E.; Ritchie, D.A.; Wiersma, D.S. Quasi-periodic distributed feedback laser. *Nat. Photon.* **2010**, *4*, 165–169. [CrossRef]
22. Biasco, S.; Ciavatti, A.; Li, L.; Davies, A.G.; Linfield, E.H.; Beere, H.; Ritchie, D.; Vitiello, M.S. Highly efficient surface-emitting semiconductor lasers exploiting quasi-crystalline distributed feedback photonic patterns. *Light Sci. Appl.* **2020**, *54*, 1–11. [CrossRef]
23. Maciá, E. Physical nature of critical modes in Fibonacci quasicrystals. *Phys. Rev. B* **1999**, *60*, 10032–10036. [CrossRef]
24. Negro, L.D.; Oton, C.J.; Gaburro, Z.; Pavesi, L.; Johnson, P.; Lagendijk, A.; Righini, R.; Colocci, M.; Wiersma, D.S. Light transport through the band-edge states of Fibonacci quasicrystals. *Phys. Rev. Lett.* **2003**, *90*, 055501. [CrossRef]
25. Ghulinyan, M.; Oton, C.J.; Negro, L.D.; Pavesi, L.; Sapienza, R.; Colocci, M.; Wiersma, D.S. Light-pulse propagation in Fibonacci quasicrystals. *Phys. Rev. B* **2005**, *71*, 094204. [CrossRef]
26. Gellermann, W.; Kohmoto, M.; Sutherland, B.; Taylor, P.C. Localization of light waves in Fibonacci dielectric multilayers. *Phys. Rev. Lett.* **1994**, *72*, 633–636. [CrossRef]
27. Hendrickson, J.; Richards, B.C.; Sweet, J.; Khitrova, G.; Poddubny, A.N.; Ivchenko, E.L.; Wegener, M.; Gibbs, H.M. Excitonic polaritons in Fibonacci quasicrystals. *Opt. Express* **2008**, *16*, 15382–15387. [CrossRef]
28. Hsueh, W.J.; Chang, C.H.; Lin, C.T. Exciton photoluminescence in resonant quasi-periodic thue–morse quantum wells. *Opt. Lett.* **2014**, *39*, 489–492. [CrossRef] [PubMed]
29. Chang, C.H.; Chen, C.H.; Tsao, C.W.; Hsueh, W.J. Superradiant modes in resonant quasi-periodic double-period quantum wells. *Opt. Express* **2015**, *23*, 11946–11951. [CrossRef] [PubMed]
30. Kohmoto, M.; Kadanoff, L.P.; Tang, C. Localization problem in one dimension: Mapping and escape. *Phys. Rev. Lett.* **1983**, *50*, 1870–1872. [CrossRef]
31. Wang, X.; Grimm, U.; Schreiber, M. Trace and antitrace maps for aperiodic sequences: Extensions and applications. *Phys. Rev. B* **2000**, *62*, 14020–14031. [CrossRef]
32. Zhang, H.F.; Liu, S.; Kong, X.K.; Bian, B.R.; Zhao, X. Properties of omnidirectional photonic band gaps in Fibonacci quasi-periodic one-dimensional superconductor photonic crystals. *Prog. Electromagn. Res. B* **2012**, *40*, 415–431. [CrossRef]
33. Rychły, J.; Mieszczak, S.; Kłos, J.W. Spin waves in planar quasicrystal of Penrose tiling. *J. Magn. Magn. Mater.* **2018**, *450*, 18–23. [CrossRef]
34. Huang, W.P. Coupled-mode theory for optical waveguides: An overview. *JOSA A* **1994**, *11*, 963–983. [CrossRef]

35. Hardy, A.; Streifer, W. Coupled mode theory of parallel waveguides. *J. Lightwave Technol.* **1985**, *3*, 1135–1146. [CrossRef]
36. Cui, L.; Zhang, S.; Lv, L.; Xu, Z.; Hayat, A.; Zhai, T. Effects of cavity coupling on 1D defect modes: A theoretical model. *OSA Contin.* **2020**, *3*, 1408–1416. [CrossRef]
37. Zhang, S.; Tong, J.; Chen, C.; Cao, F.; Liang, C.; Song, Y.; Zhai, T.; Zhang, X. Controlling the performance of polymer lasers via the cavity coupling. *Polymers* **2019**, *11*, 764. [CrossRef] [PubMed]
38. Zhang, S.; Cui, L.; Zhang, X.; Tong, J.; Zhai, T. Tunable polymer lasing in chirped cavities. *Opt. Express* **2020**, *28*, 2809–2817. [CrossRef] [PubMed]
39. Hayat, A.; Tong, J.; Chen, C.; Niu, L.; Aziz, G.; Zhai, T.; Zhang, X. Multi-wavelengh colloidal quantum dot laser in distributed feedback cavities. *Sci. China Inf. Sci.* **2020**, *63*, 1–7. [CrossRef]
40. Wong, Y.; Jia, H.; Jian, A.; Lei, D.; Abed, A.I.E.; Zhang, X. Enhancing plasmonic hot-carrier generation by strong coupling of multiple resonant modes. *Nanoscale* **2021**, *13*, 2731–3310. [CrossRef]
41. Werchner, M.; Schafer, M.; Kira, M.; Koch, S.W.; Sweet, J.; Olitzky, J.D.; Hendrickson, J.; Richards, B.C.; Khitrova, G.; Gibbs, H.M.; et al. One dimensional resonant Fibonacci quasicrystals: Noncanonical linear and canonical nonlinear effects. *Opt. Express* **2009**, *17*, 6813–6828. [CrossRef]
42. Whiteaway, J.E.A.; Garrett, B.; Thompson, G.H.B.; Collar, A.J.; Armistead, C.J.; Fice, M.J. The static and dynamic characteristics of single and multiple phase-shifted DFB laser structures. *IEEE J. Quantum Electron.* **1992**, *28*, 1277–1293. [CrossRef]
43. Zhou, Y.; Shi, Y.; Chen, X.; Li, S.; Li, J. Numerical study of an asymmetric equivalent $\frac{\lambda}{4}$ phase shift semiconductor laser for use in laser arrays. *IEEE J. Quantum Electron.* **2011**, *47*, 534–540. [CrossRef]